Kinetic and Structural Insights into the Mechanism of Binding of Sulfonamides to Human Carbonic Anhydrase by Computational and Experimental Studies

Roberto Gaspari,[†] Chris Rechlin,[‡] Andreas Heine,[‡] Giovanni Bottegoni,[†] Walter Rocchia,[†] Daniel Schwarz,[§] Jörg Bomke,[§] Hans-Dieter Gerber,[‡] Gerhard Klebe,[,‡] Andrea Cavalli,[*,†,||]*

[†]Department of Drug Discovery and Development, Istituto Italiano di Tecnologia, 16163 Genova, Italy

[‡]Department of Pharmaceutical Chemistry, Philipps-University Marburg, Marbacher Weg 6, 35032 Marburg, Germany

[§]Merck KGaA, Merck Serono Research, Small Molecule Platform/MIB, Frankfurter Str. 250, 64293 Darmstadt, Germany

[||]Department of Pharmacy and Biotechnology, University of Bologna, 40126 Bologna, Italy

[*]To whom correspondence should be addressed: GK, Klebe@Staff.Uni-Marburg.de; AC, Andrea.Cavalli@iit.it

ABSTRACT: The binding of sulfonamides to human carbonic anhydrase II (hCAII) is a complex and long-debated example of protein-ligand recognition and interaction. In this study, we investigate the para-substituted n-alkyl and hydroxyethylene-benzenesulfonamides, providing a complete reconstruction of their binding pathway to hCAII by means of large-scale molecular dynamics simulations, density functional calculations, surface plasmon resonance (SPR) measurements, and X-ray crystallography experiments. Our analysis shows that the protein-ligand association rate (k_{on}) dramatically increases with the ligand hydrophobicity, pointing to the existence of a pre-binding stage largely stabilized by a favorable packing of the ligand apolar moieties with the hCAII "hydrophobic wall". The characterization of the binding pathway allows an unprecedented understanding of the structure-kinetic relationship in hCAII/benzenesulfonamide complexes, depicting a paradigmatic scenario for the multi-step binding process in protein-ligand systems.

INTRODUCTION

Human carbonic anhydrase II (hCAII) is an enzyme that catalyzes the transformation of carbon dioxide into bicarbonate.[1,2] It is often used as a prototypical model system for biophysical studies[2,3] and medicinal chemistry applications.[2,4-6] The catalytic site of hCAII consists of one Zn^{2+} ion, which is coordinated by three histidine residues and a water molecule (or hydroxyl ion) in a distorted tetrahedral geometry.[2] Sulfonamide-carrying ligands can inhibit hCAII by directly binding to the catalytic Zn^{2+} ion of the protein and displacing the water molecule. While it is generally believed that the hCAII-sulfonamide recognition process is multi-step, little is known about the structural features of the kinetically relevant intermediate configurations along the binding pathway. As in most processes of protein-ligand binding, this can be traced back to the

transient and short-lived nature of the intermediate states, which cannot always be detected by experiments.

Our knowledge of hCAII-sulfonamide complexes relies upon extensive experimental characterization carried out over the last few decades, which has produced key results that must be taken into account when considering models of enzyme-inhibitor binding. Generally, the binding of sulfonamides to hCAII is a slow process, which considerably depends on the nature of the substituents present on the benzenesulfonamide core. This points to a multi-step mechanism, as a single-step association would be more compatible with a diffusion-limited process, characterized by fast kinetics and only marginally dependent on the chemical decorations of the binding compounds.[7,8]

The impact of the ligand substituents on the association kinetics was thoroughly investigated in the case of para-substituted n-alkyl benzenesulfonamides, where stopped-flow fluorescence (SFF) experiments[8,9] showed that the observed on-rate, k_{on}, increases exponentially with the length of the alkyl chain. These results have been interpreted in terms of a minimal two-step process, although no direct evidence of an intermediate state was produced by SFF measurements. The dissociation constants of the alkyl-substituted sulfonamides in complex with the zinc-free hCAII displayed a very high correlation with the octanol-water partition coefficient, a fact which was used to infer the key role of hydrophobic interactions in stabilizing the putative intermediate state.[9] From a structural standpoint, compounds containing alkyl chains can establish favorable interactions with the hydrophobic patch at the enzymatic cavity, often referred to as the "hydrophobic wall".[10] The role of these interactions has recently been confirmed by isothermal titration calorimetry (ITC) experiments,[11,12] molecular dynamics,[12] as

well as site-directed mutagenesis,[13-15] and X-ray crystallography data,[16-18] which are also thoroughly reviewed by De Simone et al..[19]

Further complexity to the binding mechanism is given by the charge state of the sulfonamide, which binds to the zinc ion in its anionic form, as reported by ^{15}N-NMR[20] and recent neutron diffraction studies.[21] Since benzenesulfonamides are usually weak acids, it is expected that these inhibitors initially bind to hCAII in their neutral form, and only subsequently deprotonate, upon reaching the final Zn^{2+}-coordinated configuration. On the other hand, the water molecule bound to the Zn^{2+} has a pKa value of 6.8[22] and is thought to be a hydroxyl ion in the active form of the enzyme.[3] Experimental data on the pH dependence of the association process have pointed to two possible mechanisms: either i) a neutral sulfonamide coordinates the Zn^{2+} displacing the hydroxyl ion, or ii) a charged sulfonamide displaces the Zn^{2+}-bound water molecule.[23] No consensus has yet been reached on the atomistic mechanism of sulfonamide binding to hCAII. In this scenario, the aim of this work is to provide a complete reconstruction of the binding process of para-substituted n-alkyl and hydroxylethylene-benzenesulfonamides (**1**-**5**, see Figure 1) to hCAII. The dynamical properties of the system are investigated via large-scale molecular dynamics (MD) simulations, allowing the identification of relevant pre-binding conformations adopted by compounds **1**-**5** upon their entrance into the enzyme cleft. A comparison between the predicted stability of the pre-binding conformations and the results of surface plasmon resonance (SPR) measurements is also reported. MD simulations clearly point to a multi-step binding mechanism, as previously hypothesized by Taylor, King and Burgen,[8,9] and disclose the postulated pre-binding intermediate state. The role of the hydrophobic tail mounted on the sulfonamide scaffold clearly emerges, allowing a thorough characterization of the structure-kinetics relationships (SKR) of benzenesulfonamides. We then carry out metadynamics

simulations to provide an in-depth characterization of the protein-ligand energetic landscape, which allows a description of the ligand-binding pathway up to its coordination to the Zn^{2+}-bound water, considered in our simulations as a hydroxyl ion. Subsequently, we estimate the environment-induced pKa shift of the compounds via a Poisson-Boltzmann equation-based model, and then study the sulfonamide deprotonation by means of density functional theory calculations (DFT). These results are thoroughly discussed in light of the binding models recently reviewed by Krishnamurty et al..[3] To describe the entire binding pathway, we obtain high-resolution co-crystal structures for compounds **1-5** in complex with hCAII. They unravel atomistic details of the stable Zn^{2+}-bound sulfonamide/hCAII complexes, and disclose the sulfonamide conformations as the final thermodynamic minima of the entire binding process.

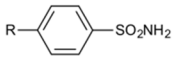

1 R = H
2 R = CH_3
3 R = CH_2-CH_3
4 R = CH_2-CH_2-CH_3
5 R = CH_2-CH_2-OH

Ligand	k_{on} (10^6 M^{-1} s^{-1})	k_{off} (s^{-1})	K_D (kinetic) (nM)	K_D (steady state) (nM)
1	1.4 ± 0.2	0.1630 ± 0.0164	1149.7 ± 101.7	1135.3 ± 196.2
2	2.0 ± 0.1	0.0582 ± 0.0073	292.9 ± 46.3	331.7 ± 93.7
3	4.7 ± 0.6	0.0461 ± 0.0033	98.3 ± 7.4	125.4 ± 25.2
4	7.8 ± 1.6	0.0454 ± 0.0129	57.8 ± 5.4	60.6 ± 5.9
5	1.6 ± 0.1	0.0643 ± 0.0079	392.0 ± 51.8	428.6 ± 55.8

Figure 1. Chemical structure and kinetic data of the para-substituted alkyl (**1-4**) and hydroxyethylene-benzenesulfonamides (**5**). The definition of the kinetic and steady-state dissociation constants (K_D) are reported in the Supporting Information.

RESULTS

The role of hydrophobicity in the structure-kinetic relationship. It was previously reported, by means of SFF investigations,[9] that the association rates for **1-4** increase exponentially with the substituent length. Here, we report SPR measurements for the same ligand series as well as for

the more hydrophilic one, compound **5**. We aim to test the effect of the methyl-hydroxyl substitution on the binding rates, to assess whether hydrophobicity or chain length is the major feature responsible for the observed k_{on} trend. The k_{on} values determined for compounds **1**-**4** (see Figure 1 and Figure 2b-c) by SPR measurements are consistent with previously reported SFF results. Although ligands **4** and **5** are of similar length, the less hydrophobic compound (**5**) displays a much smaller k_{on}. Conversely, a significant change in k_{off} is experienced between **1** and **2** only, while **2**-**5** all possess very similar dissociation rate constants. We find that the trend for the equilibrium dissociation constants K_D is driven by variation in the association kinetics, in line with the results obtained by King and Burgen.[9] Molecular dynamics (MD) simulations highlighted common hCAII-ligand interactions for the alkyl sulfonamide series (compounds **1**-**4**). In particular, we observed that the ligands approach the pocket entrance by mainly exposing the polar sulfonamide to the bulk solvent, while trying to segregate the alkyl tail in a partly exposed pocket formed by hydrophobic residues. A conformational analysis revealed the exact identity of the amino acids involved in the hydrophobic interaction, which we took as the residues having minimum distance from the ligand below 3 Å in the most populated conformational cluster. This group of residues defined a partially solvent-exposed patch (hereafter referred to as the "hydrophobic patch", HP), which grew as the size of the substituent increased (see Figure 2a and Supporting Information Figure S1). HP was largest for compound **4**, where it included amino acids I91, V121, F131, V135, L198, P201, and P202 (according to the numbering of the pdb code 1CA2),[24] and partly corresponded to the portion of hCAII known in the literature as the hCAII "secondary hydrophobic binding site"[25] (see also Figure 2a).

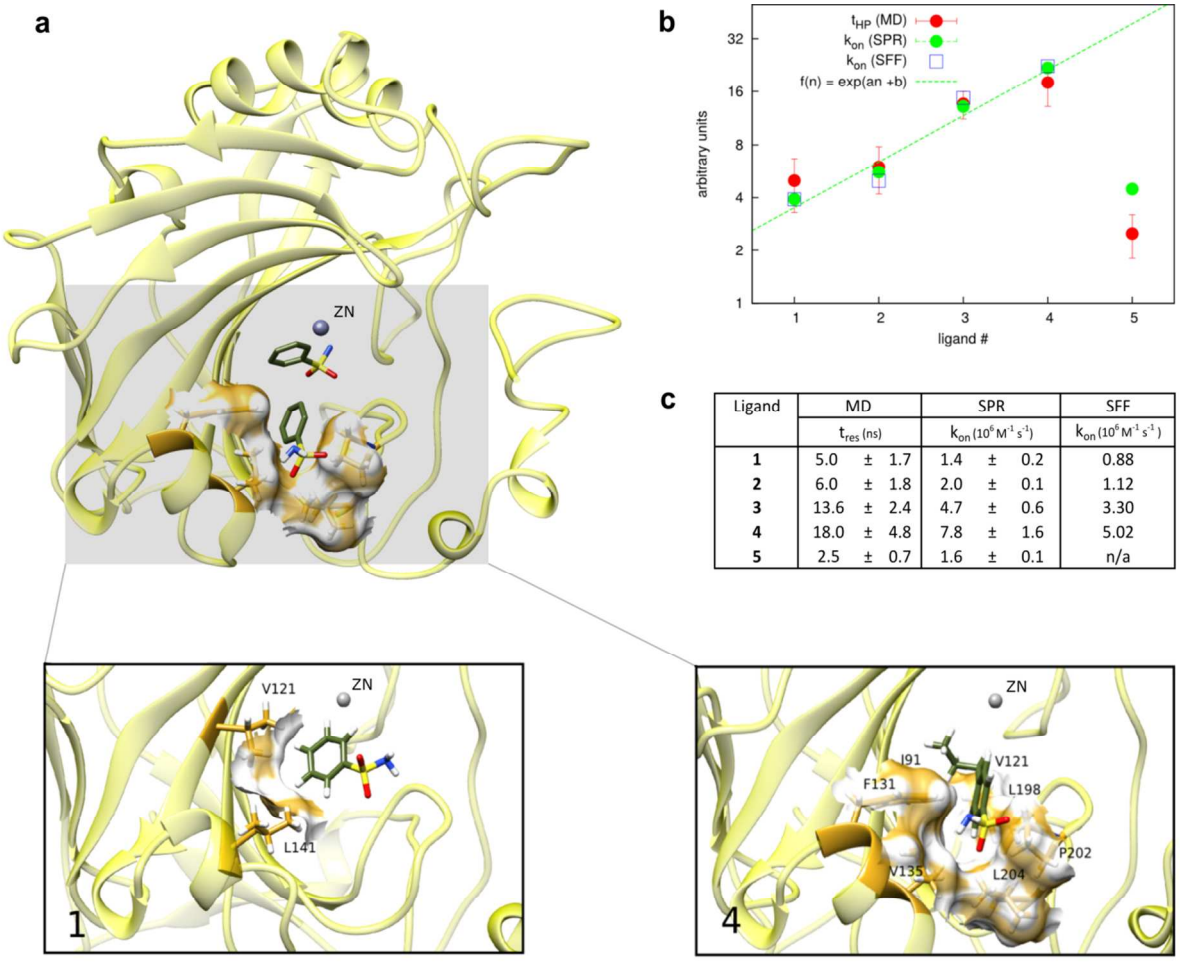

Ligand	MD	SPR	SFF
	t_{res} (ns)	k_{on} ($10^6 M^{-1} s^{-1}$)	k_{on} ($10^6 M^{-1} s^{-1}$)
1	5.0 ± 1.7	1.4 ± 0.2	0.88
2	6.0 ± 1.8	2.0 ± 0.1	1.12
3	13.6 ± 2.4	4.7 ± 0.6	3.30
4	18.0 ± 4.8	7.8 ± 1.6	5.02
5	2.5 ± 0.7	1.6 ± 0.1	n/a

Figure 2. Structure-kinetic relationships. (a) Structural overview. The clipped semi-transparent surface represents the secondary hydrophobic region at the entrance. The F conformation of the unsubstituted ligand is exemplified together with the Zn^{2+}-bound geometry, for comparison. In the inset, we represent the explicit F conformations of ligands **1**,**4** and report the hydrophobic residues with which a contact is established. (b) Comparison between the pre-binding lifetime, t_{HP} (see text), obtained in MD and the k_{on} measured by SFF and SPR experiments. Data are reported in logarithmic scale and arbitrary units on the y-axis. The green dotted line represents a linear fit on the SFF data. The variable n stands for the number of methyl/methylene groups

present in the ligand considered. (c) Table containing the mean of the actual t_{HP} and k_{on} values, reported with the standard deviation.

After binding to the HP domain, the ligand remained transiently bound to the protein and, in most of the cases, was subsequently released back into the water bulk. A quantitative description of the release process was obtained by computing, for all ligands, the lifetime of the intermediate state at the HP domain (t_{HP}). The lifetimes were computed by observing the time evolution of the minimum distance between the ligand and the HP patch, this distance being typically characterized by abrupt increases, which corresponded to ligand detachments from the protein surface (see Supporting Information). The lifetimes of **1**-**4** increased with the length of the alkyl chain as shown in Figure 2b-c. In some instances, the ligands turned the sulfonamide's polar head towards the catalytic site, reaching the hCAII catalytic pocket. We named these conformations "straight" (S), as opposed to the purely HP-bound geometries, which we labeled as "flipped" (F). Both S and F conformations could be partitioned into representative clusters (see Figure 2a, 3a and Supporting Information Figure S1). In one case (compound **1**, Figure 3a), the amide group of the sulfonamide was found to directly interact with the Zn^{2+}-bound water molecule, which is taken to be a hydroxyl ion in the present simulations. Hydrogen bond interactions between the ligands **1**-**4**, in the S conformations, and the backbone oxygen of T199 and T200 played a key stabilizing role. In addition, in the most populated S conformations, the alkyl tails of benzenesulfonamides formed favorable hydrophobic packing with the apolar side of the hCAII cavity. The largest hydrophobic cage was observed for ligand **4** and it was composed of residues V121, F131, V135, L198, and P202 (see Supporting Information Figure S1). A completely different scenario was observed with compound **5**. In the latter case, the lifetime of

the ligand on the HP patch was the shortest within the entire series (**1**-**5**, see Figure 2b-c), due to unfavorable interactions between the hydrophilic tail and HP. No buried S conformations were observed for ligand **5** during MD simulations. We could hypothesize that the transition from F to S is energetically too costly to be extensively sampled by plain MD simulation. For this reason, we resorted to so-called enhanced sampling methods (see below).

Structural characterization of the pre-binding stage. The conformational sampling was enhanced by means of metadynamics simulations within the hCAII binding cavity. We focused on the compounds displaying the most sizable structural differences, i.e. the smallest and largest ligand of the alkyl-substituted series (**1** and **4**), as well as the hydroxyl-terminated compound **5**. The free energy profile was projected over two collective variables, namely CV1 (distance between Zn^{2+} and the sulfonamide sulfur) and CV2 (angle formed by the Zn^{2+} atom, the sulfonamide sulfur and the carbon atom bound to the sulfonamide sulfur), devised to accelerate the translation (CV1) and rotation (CV2) of the sulfonamides within the cavity (see also Figure 3a). Mainly two free energy minima were found, corresponding to the S and F conformations observed in MD simulations. For all compounds, the lowest free energy minimum corresponded to S conformations characterized by a CV1 value of about 6 Å and CV2 ranging from 90° to 180°. In the energetic minimum, we found a largely visited conformation, in which the sulfonamide interacted with the Zn^{2+}-bound hydroxyl ion, showing an average distance between the sulfonamide nitrogen (N_{sulf}) and the Zn^{2+} of 3.8 ± 0.3 Å. This geometry was the one with the smallest Zn^{2+}-N_{sulf} distance obtained during our simulations, and was characterized by two hydrogen bonds between the amide group of sulfonamides and both the T200 side chain oxygen and the Zn^{2+}-bound hydroxyl. An additional hydrogen bond was observed between the sulfonamide oxygen and the T199 side chain. A pictorial representation of the S conformation is

reported in Figure 3. For ligands **1**, **4,** and **5**, we observed a secondary free energy minimum, corresponding to F conformations and well represented by the conformational clusters reported in Figure 2 and in Supporting Information Figure S2. These geometries were stabilized by a favorable hydrophobic interaction between the ligand chain and the HP patch. As for compound **5**, the free energy of the F conformation, relative to the global minimum S state, was much higher than in the case of **4**. We estimated an energy separation between the F and the S basins for **1**, **4,** and **5** of roughly 9, 12 and 22 kJ/mol, respectively (5 kJ/mol being the error estimated on convergence, see Supporting Information). In the same order, the energy of the saddle points, which divide the F from the S region, was respectively about 10, 11, and 8 kJ/mol higher than the energy of the F conformation, reflecting the energetic barrier associated with the rotation of the compound during the F to S transition. The overall free energy landscape is reported in Figure 3. Compound **5** showed an additional low free energy region, which extended approximately over the range of CV1 values between 15 and 25 Å. In the corresponding conformations, both favorable hydrophobic packing and hydrogen bonding contributed to the interaction between the ligand and the residues at the protein surface. As an explanatory example, the structure corresponding to the minimum energy of this external region is provided in Supporting Information Figure S2. Both the stability of the F conformation and the presence of the additional low energy region are expected to impact on the overall association kinetics of **5**. In Figure 3e, we report the projection of the free energy profiles of **4** and **5** on CV1. In this projection, the barrier associated with the entrance of the sulfonamide in the cavity was averaged over the rotational degrees of freedom. The hydroxyl-substituted ligand showed a substantially larger barrier than the methyl-substituted compound, pointing to the penalty due to the desolvation of **5**.

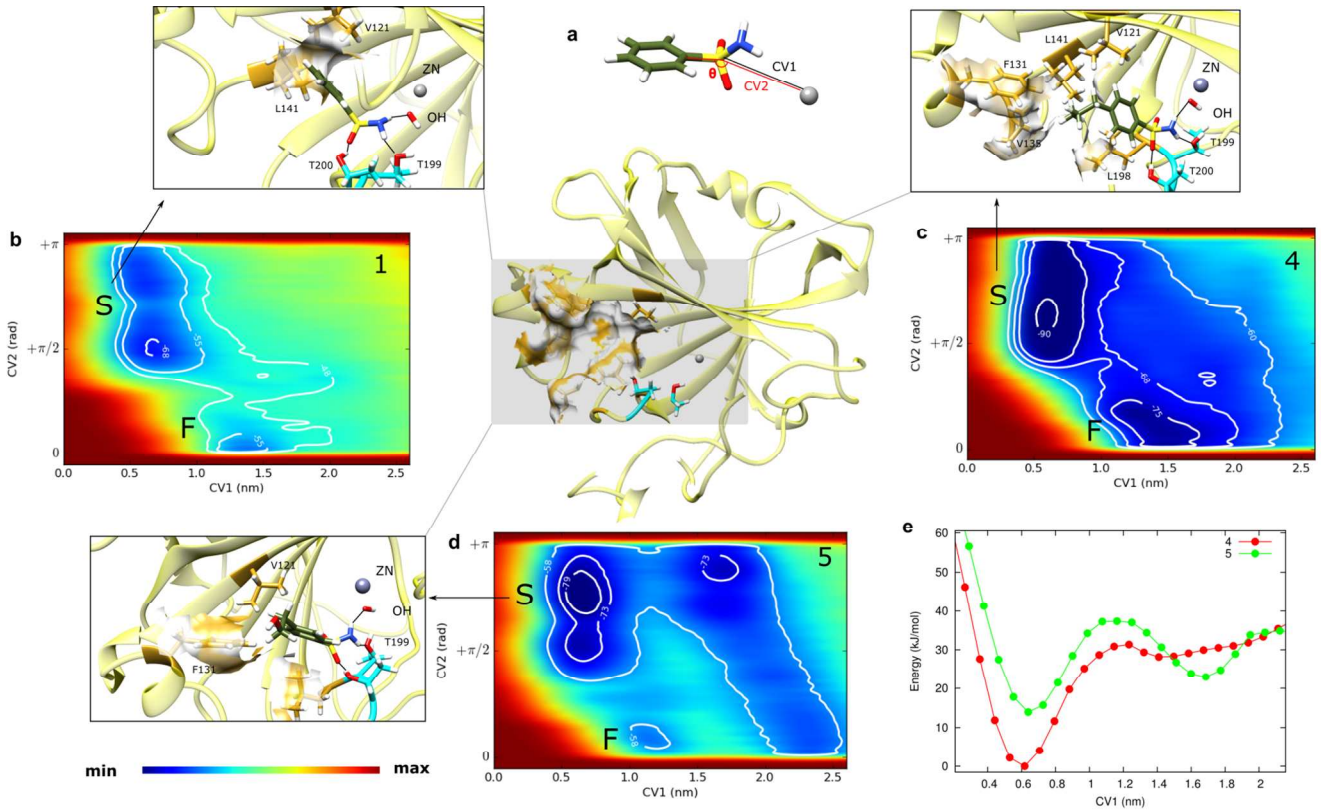

Figure 3. Free energy landscape of the protein-ligand complexes. (a) Description of CV1 and CV2 and structural overview of the protein. (b,c,d) Free energy profiles and conformations associated with the free energy minima for compounds **1** (b), **4** (c), and **5** (d). In the structural description reported in inset, the ligands and the residues within 3 Å of the S conformations are shown in stick representation. Hydrophobic and hydrophilic residues have a dark yellow and cyan skeleton, respectively. H, N, O, and S atoms are respectively white, blue, red, and yellow. In the free energy profiles, contours with the associated energy value in kJ/mol are reported. (e) Projection of the free energy profile on the CV1 for ligands **4,5** showing the different barriers associated with the two compounds.

Analysis of sulfonamide acidity. The sulfonamide moiety changes its protonation state upon binding, but the configuration where the proton-transfer mechanism occurs has not yet been identified. Therefore, we used a continuum electrostatics-based computational approach to evaluate the propensity of the sulfonamide to deprotonate in the F structures encountered during dynamics.

The approach, based on the Poisson-Boltzmann equation, yielded for the ligand **4** a pKa shift of 0.3 between the F conformation and the fully solvated structure. DFT-based geometry optimization performed on the S conformation led to a geometry in which a neutral sulfonamide forms a hydrogen bond with the Zn^{2+}-bound hydroxyl molecule. The propensity was not reversed even when the initial conformation of the system corresponded to a deprotonated sulfonamide facing a Zn^{2+}-bound water molecule. The Zn^{2+}-N_{sulf} distance at which the sulfonamide transfers one proton to the hydroxyl molecule was estimated by performing a series of DFT-based constrained geometry optimizations, in which the Zn^{2+}-N_{sulf} distance was restrained at a set of target values. The sulfonamide deprotonated spontaneously at a distance between 2.50 and 2.75 Å (see Supporting Information Figure S3).

End of the association process: crystallographic structures. The full characterization of the association process requires the knowledge of the final state, which cannot be achieved using classical MD simulations. The stable Zn^{2+}-bound conformation of the sulfonamides was instead obtained experimentally by X-ray crystallography. The geometry of the ligands in their crystallographic structure offers precious insights into the structure-kinetics relationship and the role of water networks within the protein cavity.

The crystal structures of ligands **1-5** in complex with hCAII (see Figure 4 and Supporting Information Figure S4) were determined at high resolution (hCAII-**1**: 1.01 Å, hCAII-**2**: 0.96 Å,

hCAII-**3**: 1.06 Å, hCAII-**4**: 1.08 Å, hCAII-**5**: 1.07 Å). The sulfonamide group forms with one of its oxygen atoms the typical interactions with the amide nitrogen (2.9 Å) and the side chain oxygen atom (2.8 Å) of T199.[26,27] Furthermore, the nitrogen atom of the sulfonamide coordinates to the catalytic zinc ion (2.0 Å). In Supporting Information Figure S6, we report the alignment of the common scaffold of **1**-**5**. The structure of hCAII-**1** (1.45 Å, pdb: 2WEJ) was previously published, but at a lower resolution.[26] Our structure is in good agreement with the former one, to which it adds more details, such as two additional water molecules (W7 and W8, Figure 4 and Supporting Information Figure S5). A similar structure of the water network was observed for **1**-**5**. However, a water network connecting the more buried ligand-bound waters with the solvent-exposed part of the site was only observed for ligand **1**. This aspect may play a role in the faster dissociation of **1**. A thorough discussion on the atomistic details of the water network for all ligands can be found in the Supporting Information. Additional binding configurations, stabilized by a subtle interplay of protein-ligand interactions and crystallographic packing are presented in Supporting Information Figure S6, S7 and briefly discussed in the Supporting Information**.**

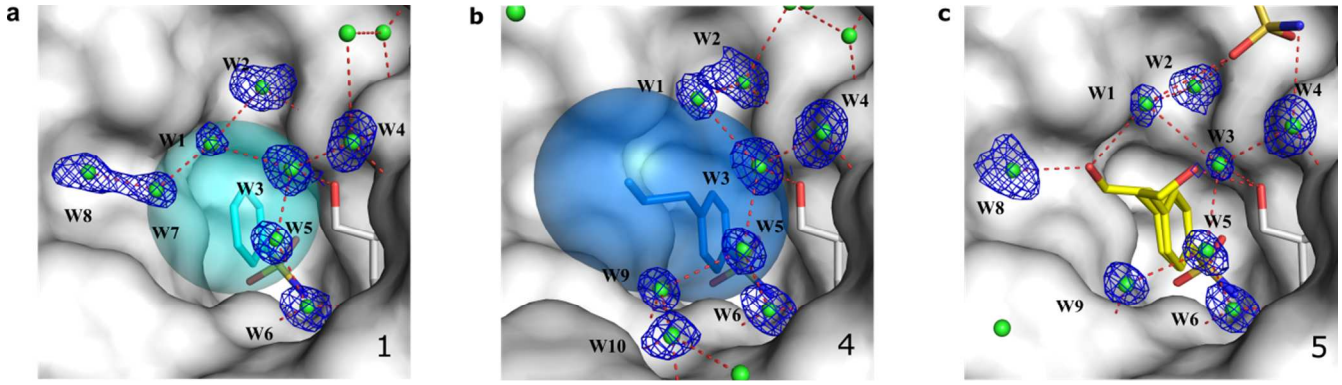

Figure 4. Crystallographic structures. Binding mode of **1** (a), **4** (b) and **5** (c) in complex with hCAII. The protein surface is shown in gray, the carbon atoms of **1, 4,** and **5** are colored in cyan, blue, and yellow, respectively. The carbon atoms of glycerol are colored in gray. Water

molecules are shown as green spheres. The $2F_o$-F_c electron density is contoured in blue at 0.50 electrons/Å^3 (0.9 σ) for water molecules W1-W8. H-bond distances (2.3 - 3.3 Å) are depicted as red-dotted lines. The Lee-Richard surfaces are shown in the same color as the carbon atoms of the respective ligands of **1** and **4**. They were generated for the hydrophobic tails of the ligands, starting with the 4-carbon atom of the phenyl ring. A contiguously connected water network, which borders the ligand at the solvent-exposed side, is detectable in the hCAII-**1** structure only. The tail of **5** is visible in two orientations.

DISCUSSION

In agreement with previous SFF data, our SPR measurements show that the association rate for ligands **1**-**4** is dependent on their chemical composition. As already discussed by Taylor, King and Burgen,[8,9] the structural dependence of k_{on} does suggest the presence of at least one intermediate state. A single-step binding process would instead be compatible with a purely diffusion-limited binding phenomenon (about 10^8 M^{-1} s^{-1} in the case of ligand-enzyme association[28]), which has not been observed for the hCAII-sulfonamides complexes considered here.

The comparison of SPR data for compound **4** and the newly analyzed compound **5** provides additional information on the nature of the binding intermediates. Compound **4** displays a considerably faster association than **5** and, since these two molecules differ only by the replacement of a methyl with a hydroxyl group in the chain, this indicates that hydrophobicity is key for the binding kinetics to this enzyme.

MD simulations support this view and show how the favorable hydrophobic packing helps to precisely stabilize the geometries along a multi-step binding pathway. Starting from the solvated

state in the bulk solution, the compounds approach the protein by ligating to an outer secondary hydrophobic site, adopting a particular conformation, named here "F conformation". As shown in Figure 2, hydrophobic packing is the only interaction that makes F conformations largely populated. Similarly, at a later stage of the binding process, the ligands adopt what we named the "S conformation", in which the apolar moieties of the compound's substituents still largely interact with the hydrophobic patch of hCAII (see Figure 3 and Supporting Information Figure S1), while the sulfonamide group is already engaged in hydrogen bonding with the protein and the Zn^{2+}-bound hydroxyl ion. Indeed, the Zn^{2+}-bound water/hydroxyl ion is an anchoring point for a wide family of ligands, which belong to the class of non-zinc binding inhibitors[2,29-35] and have been co-crystallized with hCAII in a conformation analogous to the S state here reported. For example, phenols, which are effective inhibitors of several mammalian isoforms of carbonic anhydrase,[36,37] bind to the Zn^{2+}-bound oxygen via the OH moiety, without disrupting the coordination shell of the catalytic Zn^{2+}.[30,38] Similarly, polyamines,[33,39] sulfocoumarins[34,35] and a thioxocoumarin[29] have recently been reported to directly interact with the Zn^{2+}-bound water/hydroxyl ion.

For benzenesulfomides, however, the S geometry represents a metastable state and may be regarded as the final conformation adopted by the ligand, before coordination with the Zn^{2+} ion occurs. DFT-based calculations show that the sulfonamide deprotonation can occur when the distance between the sulfonamide nitrogen and Zn^{2+} falls between 2.50 and 2.75 Å, leading finally to the displacement of the hydroxyl ion and the formation of the coordinative bond between the deprotonated sulfonamide and the enzyme's zinc ion. The structures of these final states between the sulfonamides **1**-**5** and hCAII were obtained by means of X-ray crystallography and are reported in Figure 4.

A comment is here required on the deprotonation mechanism of sulfonamides, which has remained an open issue in the literature.[3] It might be argued that sulfonamides change their protonation state before reaching the S conformation. There are, however, good reasons to consider this an unlikely hypothesis. First, in the pre-binding F conformation, the pKa value of the sulfonamide changes negligibly (0.3, according to our pKa-shift estimate), which makes a deprotonation event in the F conformation very unlikely. Secondly, the approach to the catalytic Zn^{2+}, as observed in the S conformation, does not make the sulfonamide acidic enough for a proton transfer. Indeed, DFT geometry optimizations predict that the proton transfer from the sulfonamide to the hydroxyl ion cannot occur spontaneously in the S conformation, requiring a shorter distance between the sulfonamide group and the Zn^{2+}. Therefore, the present computational study points to a mechanism in which the sulfonamides approach hCAII in their neutral state, bind to the hydrophobic patch, and interact with the Zn^{2+}. Then, only if the distance between their terminal NH_2 group and the Zn^{2+} is about 2.50-2.75 Å, will they get deprotonated and coordinate the Zn^{2+} ion, resulting in the final thermodynamic minimum.

Overall, our analysis, at least for the alkyl-substituted derivatives (compounds **1**-**4**), suggests a three-step process, regulated by partial kinetic constants as described as described in Figure 5 and in the scheme below:

$$[P][L] \underset{k_{-1}}{\overset{k_1}{\rightleftarrows}} [F] \underset{k_{-2}}{\overset{k_2}{\rightleftarrows}} [S] \overset{k_3}{\longrightarrow} [PL] \qquad (1)$$

where [P][L] represents the unbound protein-ligand system, [F] and [S] correspond to the previously discussed conformations, and [PL] stands for the Zn^{2+}-bound sulfonamide complex. We can get an insight into the dependence between the partial kinetic constants and the observed k_{on} by first considering the conversion between [P][L] and [F] as a rapid pre-equilibration step. This is justified by the analysis of our MD simulations, showing that $k_{-1} \gg k_2$. Secondly, if we

assume the change in concentration of [S] will be small, i.e. we apply steady-state kinetics for the second and third step, we reveal the following overall association constant (see Supporting Information for a simple derivation) as:

$$k_{on} = (k_1/k_{-1}) \cdot (k_2 k_3/(k_{-2} + k_3) \qquad (2)$$

In the derivation we set $k_{-3} = 0$, similarly to what done by King and Burgen[8,9] for the dissociation step in the simpler two-state mechanism.

The rate associated with the ligand diffusion, k_1, as well as the deprotonation rate, k_3, may be considered weakly dependent on the chemical decoration throughout the ligand series **1**-**4**. Actually, k_1 is determined by the Brownian diffusion of the ligand in solution and only weakly depends on the hydrodynamic radius of the molecule, which remains nearly constant across the series **1**-**4**. Similarly, changes in the substituents within the ligands investigated occur rather remote from the sulfonamide group and are not expected to largely influence the amide group acidity. Actually, in bulk water, the pKa difference between **1** and **4** is about 0.2.[8,9] Moreover, the barriers for conversion between the F and S conformations are predicted to be similar (see Figure 3), at least for the alkyl-substituted ligands. Inspired by these considerations, we conjecture that the k_{on} trend along **1**-**4** should mainly correlate with the inverse of the partial unbinding rate k_{-1}, which can be estimated by the lifetimes of the ligands at the hydrophobic patch (HP). The explicit calculation of t_{HP} (see Figure 2) supports our hypothesis. The release kinetics, described by k_{-1}, of the intermediate complex F also provides an explanation for the exponential dependence of k_{on} on the alkyl chain length, for the ligand series **1**-**4**. Adding one methylene group to the alkyl chain energetically stabilizes the F structures by an amount, ΔG_{CH2}, which represents the free energy penalty associated with the transfer of one methylene group from the protein's apolar environment to the water solution. By adopting a simple Arrhenius relationship, the rate k_{-1} decreases by a factor $\exp(-\beta\Delta G_{CH2})$ when a methylene group is added to

the substituent chain. The fit of the Arrhenius expression to the SFF data leads to a value of ΔG_{CH2} of 1.56 ± 0.25 kJ/mol (see Figure 2b). The free energy penalty, per CH_2 group, associated with the transfer of an alkyl chain from a lipophilic to aqueous solvent was experimentally determined to be 3.35 kJ/mol.[40,41]

This value can be considered consistent with our estimation of ΔG_{CH2}, as the benzenesulfonamides desorb from a hydrophobic surface (rather than from a bulk hydrophobic solution), which was in contact with approximately one half of the total volume occupied by the alkyl chain.

The experimental k_{off} values, obtained by SPR experiments, are nearly independent of the compound structures, in agreement with previous SFF results.[8,9] The notable exception is ligand **1**, the k_{off} of which is nearly three times bigger than that measured for the other compounds. The crystal structure of **1** in complex with hCAII shows a unique arrangement of crystallographic waters compared to the other derivative, which fully surround the ligand and connect it to the solvent exposed side. This could indicate the crucial role of a water network in the observed k_{off} value. On the other hand, hydrophobicity does not play a role in determining the off rates: the presence of the hydroxyl group in **5** does not lead to a dramatic reduction in the k_{off} with respect to the similarly sized ligand **4**.

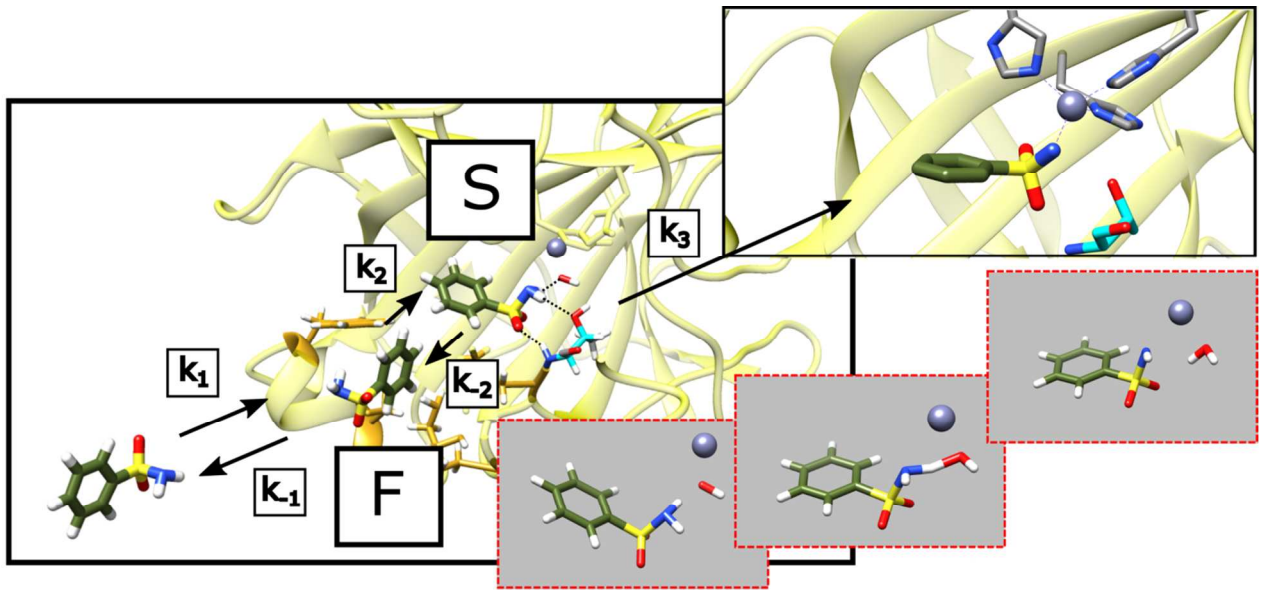

Figure 5. Overview of the binding process. The unbound ligand approaches the protein and reaches the F conformation, located in the external hydrophobic patch, with rate k_1. At this stage, the ligand might return to the unbound state with rate k_{-1} or reach the S conformation with rate k_2. From the S state, characterized by geometries displaying hydrogen bonding with T199, T200, and the Zn^{2+}-bound hydroxyl ion, the compound can possibly leave the site with rate k_{-2} or reach the final crystallographic structure (see inset) with rate k_3. Final isomerization to the Zn^{2+}-bound pose requires deprotonation of the sulfonamide moiety and conversion of the Zn^{2+}-bound hydroxyl ion to a water molecule. The proton transfer mechanism is sketched in the sequence of bottom right insets.

CONCLUSIONS

In this work, we have performed an in-depth characterization of the structure-kinetic relationship of sulfonamide-bearing compounds and hCAII, using a combination of experimental and simulative techniques, including SPR, X-ray crystallography as well as MD, metadynamics,

Poisson-Boltzmann and DFT calculations. As evidenced by the SPR results, the affinity of benzenesulfonamides for the hCAII target appears to be mostly modulated by changes in the association rate, while, in turn, the association rate trends are dictated by the compound hydrophobicity. Large-scale MD and metadynamics simulations explain the role of hydrophobicity, by pointing to the existence of well-defined pre-binding conformations along a multi-step binding pathway. A specific prebinding conformation, stabilized by a favorable packing of the compound apolar moieties with a secondary hCAII hydrophobic patch, displays a disruption rate, k_{-1}, which dramatically decreases with the ligand hydrophobicity. According to the classical rate theories, this result explains the trend of the association rates in the n-alkyl benzenesulfonamide compounds, whose k_{on}, according to previous SFF measurements and in agreement with our SPR results, depends exponentially on the alkyl chain length. DFT and pKa shift calculations indicate that sulfonamides enter the protein pocket in the neutral form and reach the anionic form only at close proximity of the Zn^{2+} catalytic ion, prior binding to the Zn^{2+} ion in the conformation shown by the high resolution X-ray structures. These structures also highlight a complex water network surrounding the compounds substituents. This information allows a rational understanding of the binding kinetics of sulfonamide-hCAII complexes and lays the basis for further investigations of the structure-kinetics relationship in a large class of highly non-trivial binding mechanisms, where an early slow recognition process must be taken into account along with a proton transfer reaction. We believe that our work offers a paradigmatic approach, showing how the combination of several experimental and simulative methods can be generally used to produce a detailed understanding of the enzyme-inhibitor recognition and binding mechanisms.

EXPERIMENTAL SECTION

Computational Methods.

Protein preparation. hCAII coordinates were retrieved from the Protein Data Bank (pdb: 1CA2).[24] Amber99sb[42] force field was used for modeling the standard residues. The catalytic site was described by the Zinc Amber Force Field (ZAFF) force field.[43] The crystallographic water bound to the zinc ion was assumed to be a hydroxyl ion.

Ligand preparation. Ligands **1-5** (Figure 1) were parameterized using the Generalized Amber Force Field (GAFF).[44] Charges were refitted by means of restrained electrostatic potential (RESP).[45] The three lowest energy structures, obtained by *in-vacuo* conformational search using Macromodel[46] and employing the Optimized Potential for Liquid Systems[47,48] (OPLS), were used for charge fitting.

Molecular dynamics and metadynamics simulations. MD simulations were run for 1 μs (**1**) 1.2 μs (**2**) 1.1 μs (**3**) 1.1 μs (**4**) 1 μs (**5**) using the Gromacs 4.5.5 package.[49] Simulations were run in the NPT ensemble, using the Parrinello-Rahman barostat[50] with time constant τ = 2 ps and the V-rescale thermostat[51] with time constant τ = 0.1 ps. A time step dt = 2 fs was used. Geometry optimization was performed on the initial conformation up to a force threshold of 10 kJ· mol^{-1} ·$Å^{-1}$ and the resulting structure was brought from 0 to 300 K using a constant annealing of 400 ps. Well-tempered metadynamics[52] simulations were performed on (**1,4,5**) using the PLUMED plugin.[53] The duration of each run was at least 150 ns per ligand. We used two collective variables, CV1 and CV2 defined as the Zn-S1 distance and the Zn-S1-C1 angle, S1 and C1 representing, respectively, the sulfur of the sulfonamide and the carbon bound to it (see also Figure 3a). The initial Gaussian height was set to 2.5 kJ mol^{-1}, while Gaussian widths were set to

2.5 Å and 0.5 rad for CV1 and CV2, respectively. The Gaussian deposition time interval was set to 2 ps. The CV fictitious temperature was set to 1200 K. Simulations were stopped after at least 5 recrossings from the lowest free energy conformation. This allowed the difference between the minima of the free energy profiles to remain constant within 5 kJ· mol^{-1} over the final 25 ns of the simulation.

Definition of the simulation region. We defined a simulation region as an ensemble of spheres with a 5 Å radius, centered on each atom of the following residue group: W5, W16, F20, P21, I22, I91, V121, W123, F131, V135, L141, A142, V143, L198, P201, P202, L203, L204, and W209. We considered the following minimum distance collective variable:

$$s = \frac{\beta}{log\sum_{ij} exp\left(\beta / \| r_{ij} \|\right)} \quad (3)$$

Where $\|r_{ij}\|$ represents the distance between the *i-th* atom of the ligand and the *j-th* atom of the residue group. β was set to 500.

The constraining potential was introduced as:

$$U(s) = 0 \; for \; s < s_0 \quad (4)$$

$$U(s) = k(s - s_0)^4 \; for \; s \geq s_0$$

where s_0 = 5 Å and k=$4 \cdot 10^2$ kJ · $mol^{-1} \cdot Å^{-1}$. Using these conditions, the ligand, when lying completely outside of the confining region, experiences a restraining force, preventing the escape of the ligand itself from the confinement volume. This allows sampling of a larger number of detachment events with respect to unconfined simulations, without biasing the dynamics during the event of ligand desorption. The shape of the constraining region as it appears in the hCAII crystal structure is displayed in Figure S8. Because of the relatively large Gaussian width employed, metadynamics simulations were allowed to sample a larger volume, i.e. the spheres used to define the simulation region were set to 10 Å.

Pre-binding lifetime. The individual lifetimes, t_{HP}, of ligands on a predefined hydrophobic patch were computed by monitoring the time evolution of the minimum distance *s* between the ligand atoms and all the atoms of the patch. The considered patch need not be the whole restraining region defined above, but could be a portion of it, as specified in the main text (see definition of HP patch). In our calculations, the actual region used for lifetime calculations was the union of the HP patches for the ligands **1**-**4**, corresponding to a pocket comprising I91, V121, F131, V135, L141, L198, P201, and P202. This choice allowed us to focus on the lifetime of the relevant pre-binding conformations, which are stabilized by hydrophobic interactions and are precisely hosted in the above-mentioned patch. Two threshold values, s_{low} and s_{high}, were introduced and used to tag the state as "adsorbed" (A) or "desorbed" (D) following four classification rules:

At time t=0, State(0)=D if $s(0) > s_{low}$ or State(0)=A if $s(0) < s_{low}$.

At any time t_0 such that: $State(t_0\text{-}dt) = A$ and $s(t_0) > s_{high}$, then: $State(t_0) = D$.

At any time t_0 such that: $State(t_0\text{-}dt) = D$ and $s(t_0) < s_{low}$, then: $State(t_0) = A$.

In all other cases $State(t_0) = State(t_0\text{-}dt)$

In our calculations, we used s_{low}=2 Å and s_{high}=5 Å. The first value can be considered the distance at which a hydrophobic contact between the ligand and the HP patch is actually established. The second value corresponds to a rather minimal distance at which the ligand and the patch can be separated by a water molecule. The total length of an adsorption event defines the individual lifetime, t_{HP}. At least 20 desorption processes per ligand have always been

observed. The procedure to compute t_{HP} is exemplified in Figure S9. The distributions of the lifetimes are reported for all ligands in Figure S10.

Conformational cluster analysis was performed using the Gromos method.[54] The RMSD cutoff radius employed was 2 Å, and atoms included in the RMSD calculation were the *Cα* of the residues in the restraining patch and the ligands' atoms.

Poisson-Boltzmann calculations. A thermodynamic cycle was considered, connecting the protonated and deprotonated sulfonamide molecules in aqueous solvent, where the pKa is known experimentally, and the same compounds once in the presence of the hCAII protein at a desired location. Considering the overall low charge of the system, the linearized Poisson-Boltzmann equation was solved for each of the four systems by means of the finite differences method provided by the DelPhi v.4 code.[55] The grid spacing was set to 0.5 Å and particular care was devoted to maintaining the same relative position of the sulfonamides with the finite differences grid in all the simulations. Coulombic-type boundary conditions and a percentage filling of 70% were used. The pKa shift was obtained by considering the difference between the electrostatic energy of protonated and deprotonated forms in the presence and absence of the protein.

DFT calculations. Calculations were performed on two systems (1,2) constructed as follows. (1): the S conformation was taken from dynamics for ligand **1** and optimized up to a force threshold of 10 kJ · mol^{-1} $Å^{-1}$. We then selected the residues coordinating the ligand, resulting in a system comprising H94, H96, H119, H64, E106, T199, and T200. In the reduced model used, the residues have been cut at C_β and one extra hydrogen was added to complete the coordination of the C_β. All waters found within 4 Å of the ligand were included in the calculation. (2): system (1) was modified by translating the H atom involved in the H-bond between the sulfonamide and

the Zn^{2+}-bound hydroxyl ion along the H-O bonding distance. The resulting conformation corresponded to a Zn^{2+}-bound water molecule facing the deprotonated sulfonamide.

Both systems were structurally optimized up to a force threshold of $4.5 \cdot 10^{-4}$ atomic units. In (1) and (2), all the C_β and the oxygen atoms of the water molecules with truncated coordination were kept fixed during DFT geometry optimization. In (2), the geometry was optimized by first fixing the sulfonamide nitrogen and the transferred hydrogen, and by then relaxing the whole system. All electron DFT calculations were performed using the CRYSTAL14 codes.[56] Basis sets were taken from the crystal website library.[57]

Constrained geometry optimization was performed by applying an external harmonic force between the sulfonamide nitrogen and the Zn^{2+} ion. The spring stiffness was set to 0.5 atomic units. Starting from the DFT-optimized S pose, the equilibrium length of the spring was gradually brought to 2.0 Å in ten steps. Each step corresponded to a new geometry optimization, with input coordinates taken from the system optimized at the previous iteration. At each step, the equilibrium length was reduced by 0.25 Å. The CP2K code[58] was used for the constrained geometry optimizations. The force threshold for structural optimization was set to $4.5 \cdot 10^{-4}$ atomic units. Goedecker-Teter-Hutter pseudopotentials[59] were used for all elements. All the electrons in the highest energy electronic shell were considered as valence electrons. In the case of Zn, the semicore 3d electrons were also included. Double zeta valence basis sets with one polarization function[60] were used. A structural analysis of the deprotonation process can found in the Supporting Information.

Experimental Methods.

Expression and purification of hCAII. 100 ml LB media containing 100 µg/mL ampicillin (Roth) and 34 µg/mL chloramphenicol (Roth) were inoculated with BL21 Codon Plus cells containing a pGEX-4T1 (GE Healthcare) plasmid with the sequence of the hCAII-glutathione-S-transferase fusion protein. After shaking with 200 rpm for 16 h at 310 K, 25 mL of this overnight culture were transferred into 1L LB media (with 100 µg/mL ampicillin). At an OD_{600} of 0.6-0.8, 1mL of a 2 M IPTG solution was added. After 4 h at 305 K, the cell suspension was centrifuged at 5000 rpm. The cells were resuspended in PBS buffer (139.3 mMNaCl, 2.7 mMKCl, 10.0 mM Na_2HPO_4,1.8mM KH_2PO_4) and the cell walls were disrupted using ultrasound. The suspension was centrifuged at 20.000 rpm. A column which was filled with 20 mL glutathione sepharose high performance material (GE Healthcare) was equilibrated with reduced glutathione (Sigma Aldrich) followed by PBS buffer and afterwards loaded with the supernatant. The column was washed with 500 ml PBS buffer. Afterwards a solution of thrombin (CSL Behring, Marburg) was injected onto the column. Overnight, the fusion protein was cleaved on the column. The released hCAII was washed from the column with PBS buffer. To remove the thrombin, a HiTrap 1mL Benzamidine FF column (GE Healthcare) was used. A final purification step with a HiLoad 26/600 Superdex 200 pg size exclusion column (Amersham Biosciences) which was equilibrated with 50 mMTris buffer (pH 7.8) was performed. The purity of the protein was analyzed by SDS gel electrophoresis.

Ligands. The ligands **1**, **2**, 4-CBS (**6**) and sulfanilamide (**7**) were purchased from Sigma Aldrich. 3was purchased from Apollo Scientific Ltd., **4** and **5** from Ukrorgsyntez Ltd. (UORSY).

Ligand verification and purification. All 4-substituted benzenesulfonamides (**1-5,** reference ligands **6,7**) were commercially obtained. Except for compound **5**, all substances had at least a stated purity of 95% or higher, which was also verified by ^{1}H NMR spectroscopy, elemental

combustion analysis, and ESI mass spectroscopy. The respective experimental data are described in the Supporting Information section.

Due to a rather poor quality of the commercial batch of 4-hydroxyethyl-substituted benzenesulfonamide **5** (85%) as indicated by quantitative ^{1}H NMR spectroscopy and elemental combustion analysis, the compound initially rendered inconsistent assay results. Therefore, purification of this compound was performed applying two consecutive column chromatography steps leading to significantly improved purities of 94% (first purification step) and 98% (second purification step), respectively, as determined by quantitative ^{1}H NMR experiments (see Supporting Information). In the following, the purified batches delivered conclusive assay data.

SPR. The measurements were performed on a Biacore S51 device (GE Healthcare, Uppsala). For immobilization, PBS buffer (139.3 mMNaCl, 2.7 mMKCl, 10.0 mM Na2HPO4, 1.8 mM KH2PO4) with 0.05% Tween 20, pH 7.4, was used as a background buffer. The standard amine coupling procedure was applied. A series S Sensor Chip CM5 was activated with a mixture of 0.1 M NHS (N-hydroxysuccinimide) and 0.4 M EDC (1-ethyl-3-(3-dimethylaminopropyl) carbodiimide- hydrochloride) at a flow rate of 10 µL/min for 10 minutes. Then, a 50 µg/mL solution of hCAII in 10 mM sodium acetate (pH 5.2) with 30 µM ethoxzolamide was injected for 2 minutes followed by an injection of 1 M ethanolamine hydrochloride (pH 8.5) for 7 minutes. This procedure led to immobilization levels between 3500 and 4900 RU. For measuring the compounds, PBS buffer with 0.05% Tween 20 and 2% DMSO, pH 7.4, was used as the running buffer. The compounds were injected at a flow rate of 30 µL/min for 120 s. Then, the dissociation was monitored for 300 s. No regeneration was needed since all the investigated compounds completely dissociated from the sensor chip surface in the applied time window. In total, 10 concentrations were investigated for each compound in a twofold dilution series. For the

different compounds, the following concentrations were measured: **1** (19.5 nM-10.0 μM), **2** (9.8 nM - 5.0 μM), **3** (3.9 nM- 2.0 μM), **4** (1.2 nM- 600 nM), **5** (9.8 nM – 5.0 μM), 4-CBS (31.3 nM-16 μM), and sufanilamide (273.4 nM- 140.0 μM). A solvent correction cycle using DMSO concentrations between 1.4 – 2.8% was run in between every two sample concentration series. The data were evaluated with the Biacore S51 evaluation software (version: 1.2.1). The signals of the reference spot were subtracted from the signals of the measurement spots. Then, the sensorgrams were corrected for mismatches in the DMSO concentrations. Two blank injections, carried out contemporary to the injections of the respective ligand, were subtracted from the sensorgrams. For each single measurement, the most robust method for fitting was chosen with a global maximum response (R_{max}) and a constant value of 0 for the shift of the refractive index (RI) at the beginning and end of each injection. The kinetic parameters k_{on} and k_{off} were obtained using a simple 1:1 interaction model including a term for a mass transfer limitation as implemented in the evaluation software. The test for a mass transfer limitation as implemented in the evaluation software showed that the curve that was fitted into the sensorgrams was not mass-transfer-limited. Thus, the obtained kinetic constants of our final results were reliable. K_D (kinetic) was obtained by k_{off}/k_{on}. K_D (steady state) was obtained by plotting the binding level at the end of each injection against the concentration of the compound and fitting it to a single-site binding isotherm. The ligands **1**-**5** were measured one after another at four independent protein surfaces of 3700 RU, 3600 RU, 4900 RU, and 4700 RU. The ligands 4-CBS, sulfanilamide, **5** (94%), and **5** (98%) were measured consecutively at four independent protein surfaces of 4900 RU, 4800 RU, 4500 RU, and 4500 RU. In Table S1, the results of the single measurements of **1**-**5** are listed. An example curve for each ligand is presented in Figure S11. In preliminary tests, an impurity was discovered for compound **5**. It was purified to at least 94% in the first sample; a

second purification step provided 98% purity. Two dilution series, one with the substance with 94% purity and a second based on 98% purity, were measured in four independent SPR experiments and the kinetic parameters for the binding to hCAII were determined. As shown in Table S2, the results are very similar for both purity levels. Thus, the reduced purity of **5** (94%) compared to the ligands **1**-**4** does not explain the deviating kinetic parameters.

We validated our assay by measuring 4-CBS (**6**) and sulfanilamide (**7**) as reference ligands and comparing our results with previously determined values by Myska[61] for the binding of these compounds to the bovine CAII (bCAII). Both compounds possess a very similar chemical structure compared to **1**-**5**. Two independent series of measurements with hCAII immobilized on both spots were performed so that four single measurements on four independent hCAII-surfaces could be taken on two consecutive days. Table S3 lists the results of the single measurements, the mean values, and the corresponding standard deviations. Although we worked with human CAII, we were able to measure similar affinity data for 4-CBS (hCAII: 0.89 µM, bCAII: 0.89 µM) and sulfanilamide (hCAII: 5.55 µM, bCAII: 5.88) as described in the literature for the bovine type. Furthermore, the kinetic constants show a similar trend, identifying 4-CBS (k_{on} hCAII: $6.5 \cdot 10^4$ $M^{-1}s^{-1}$; k_{on} bCAII: $4.1 \cdot 10^4$ $M^{-1}s^{-1}$; k_{off} hCAII: 0.0575 s^{-1}; k_{off} bCAII: 0.0369 s^{-1}) as the compound with the faster association and slower dissociation with respect to sulfanilamide (k_{on} hCAII: $3.7 \cdot 10^4$ $M^{-1}s^{-1}$; k_{on} bCAII: $2.3 \cdot 10^4$ $M^{-1}s^{-1}$; k_{off} hCAII: 0.2053 s^{-1}; k_{off} bCAII: 0.1330 s^{-1}). Additionally, this series of measurement showed that the assay was reproducible when similar amounts of protein were immobilized on the sensor chip.

The running buffer in an SPR experiment often contains 0.005 - 0.05% Tween 20 to prevent unspecific binding to the tubings and other hydrophobic parts of the instruments. To exclude the possibility that Tween 20 interferes with the binding of ligands **1**-**5** to hCAII, the same series of

measurements were performed twice with the same protein surface, once with 0.05% Tween 20 in the running buffer and once without the detergent. The results are listed in Table S4. Similar values were obtained for ligands **2**-**5** in both cases. Ligand **1** showed sensorgrams which did not reach saturation when Tween 20 was not added. Thus, we did not evaluate the data for **1** in this case. The other ligands showed similar results in both cases. Since **1** showed a satisfying saturation when adding 0.05% Tween 20, the measurements were done in the presence of the tenside. For the final measurements of the investigated ligand series (**1**-**5**), single measurements on four independent protein surfaces were performed. The results of the single measurements are listed in Table S1. The mean values and the standard deviations are shown in the main text in Figure 1. To partially average out the small variation of the kinetic constants depending on the immobilization level, we decided to determine the mean of these four surfaces exhibiting different protein densities. We performed experiments with immobilization levels at a lower rate corresponding to 1000 RU. However, the quality of the obtained sensorgrams was not sufficient. Our results are not significantly influenced by a mass-transfer limitation even at a high immobilization level. Thus, the applied immobilization levels were chosen since they led to a good signal-to-noise ratio.

Crystallization and soaking. The concentration of hCAII in 50 mMTris pH 7.8 was adjusted to 10 mg/mL. 2.5 μL of this solution was mixed with 2.5 μL of the well solution (2.7 M $(NH_4)2SO_4$, 100 mMTris, saturated with p-chloromercurybenzoic acid) and placed as a hanging drop. Crystals appeared overnight and reached their full size after 2 weeks. The crystals were soaked with a saturated solution of the inhibitor in a stabilization buffer (3.0 M $(NH_4)2SO_4$, 100 mMTris) for one day. Afterwards they were rapidly dipped in the cryo buffer (2.7 M $(NH_4)2SO_4$,

100 mMTris, 25% V/V glycerol, 1mM of the respective inhibitor, 1% V/V DMSO) for a short time and subsequently frozen in liquid nitrogen.

Data collection, processing and refinement. All data sets were collected at beam line 14.1 at the synchrotron BESSY II (Berlin-Adlerhof, HZB, Germany[62]). The data sets were processed and scaled using XDS.[63] Molecular replacement was done using Phaser[64] from the CCP4 suite[65] using pdb entry 1CNI as a starting model.[66] 5% of the reflections were marked for the calculation of the R_{free} value. In the Phenix suite[67] the program phenix.refine (version 1.8.4-1492) was used to perform three cycles of rigid body refinement and five cycles of Cartesian simulated annealing followed by five cycles of minimization. Then, alternating cycles of model building in Coot[68] and refinement in Phenix were performed. Single atoms of side chains of amino acids were deleted if they were not clearly visible in the 2Fo-Fc electronic density at 1.0σ. Water molecules were only placed when indicated by the Fo-Fc difference electron density at 3.0. The tails of ligands **3**, **4**, and **5** were not immediately visible. After assigning the core structure of the respective ligand to the density, they became visible atom by atom in following minimization cycles in the Fo-Fc electronic density maps at 3.0σ. An anisotropic refinement of the temperature factors for all atoms except hydrogens was performed. The coordinates and restraints for the ligands and for p-chloromercurybenzoic acid were built using Grade.[69] Finally, hydrogen atoms were added to the model using the riding model. However, the R_{free} value did not improve significantly. Thus, we refrained from adding hydrogen atoms to the final model. Validation was performed using MolProbity[67] as implemented in the Phenix suite and PROCHECK.[70] 2Fo-Fc electron density maps for the ligands are shown in Figure S12. The coordinates were deposited in the PDB (hCAII-**1**: 4YX4, hCAII-**2**: 4YXI, hCAII-**3**: 4YXO, hCAII-**4**: 4YXU, hCAII-**5**: 4YYT). Statistics for data collection, processing, and refinement are shown in Table S5.

ASSOCIATED CONTENT

Supporting Information. Additional experimental details; alternative binding conformations; comparison of the crystallographic structure for ligand 1 with the previously published 2WEJ; description of the crystallographic water network; derivation of rate equations; details of the ligands purification; Figures S1 – S12; Table S1 – S5;

Accession codes. hCAII-**1**: 4YX4, hCAII-**2**: 4YXI, hCAII-**3**: 4YXO, hCAII-**4**: 4YXU, hCAII-**5**: 4YYT.

AUTHOR INFORMATION

Corresponding Authors: *E-mail: Klebe@Staff.Uni-Marburg.de, Tel.: +49-6421-28-21313; *E-mail: Andrea.Cavalli@iit.it, Tel.: +39-051-20-9-9735.

Notes: The authors declare no competing financial interests.

ACKNOWLEDGMENTS

We are grateful to the beamline staff at BESSY II (Helmholtz-Zentrum Berlin) in Berlin, Germany for providing us with outstanding support during the data collection and the Helmholtz-Zentrum Berlin for travel support. The present study was kindly supported by the ERC Advanced Grant no. 268145-DrugProfilBind awarded to GK. The supercomputer center CINECA is gratefully acknowledged for providing us with CPU time and for the overall support. We thank Grace Fox for proofreading the manuscript.

ABBREVIATIONS USED

hCAII, human carbonic anhydrase II; SPR, surface plasmon resonance; SFF, stopped flow fluorescence; ITC, isothermal titration calorimetry; SKR, structure-kinetics relationships; k_{on}, ligand association rate; k_{off}, ligand dissociation rate; K_D, dissociation constant; HP, hydrophobic patch; t_{HP}, lifetime of the intermediate state at the hydrophobic patch; S conformation, straight conformation; F conformation, flipped conformation; CV, collective variable.

REFERENCES

1. Tripp, B. C.; Smith, K.; Ferry, J. G. Carbonic Anhydrase: New Insights for an Ancient Enzyme. *Journal of Biological Chemistry* **2001,** 276, 48615-48618.
2. Alterio, V.; Di Fiore, A.; D'Ambrosio, K.; Supuran, C. T.; De Simone, G. Multiple Binding Modes of Inhibitors to Carbonic Anhydrases: How to Design Specific Drugs Targeting 15 Different Isoforms? *Chemical Reviews* **2012,** 112, 4421-4468.
3. Krishnamurthy, V. M.; Kaufman, G. K.; Urbach, A. R.; Gitlin, I.; Gudiksen, K. L.; Weibel, D. B.; Whitesides, G. M. Carbonic Anhydrase as a Model for Biophysical and Physical-Organic Studies of Proteins and Protein−Ligand Binding. *Chemical Reviews* **2008,** 108, 946-1051.
4. Supuran, C. T. Carbonic anhydrases: novel therapeutic applications for inhibitors and activators. *Nature Reviews: Drug Discovery* **2008,** 7, 168-181.
5. Supuran, C. T.; Scozzafava, A. Carbonic anhydrases as targets for medicinal chemistry. *Bioorg Med Chem* **2007,** 15, 4336-4350.
6. Aggarwal, M.; McKenna, R. Update on carbonic anhydrase inhibitors: a patent review (2008 – 2011). *Expert Opinion on Therapeutic Patents* **2012,** 22, 903-915.
7. King, R. W.; Burgen, A. S. V. Kinetic Aspects of Structure-Activity Relations: The Binding of Sulphonamides by Carbonic Anhydrase. *Proc. R. Soc. B* **1976,** 193, 107-125.
8. Taylor, P. W.; King, R. W.; Burgen, A. S. Kinetics of complex formation between human carbonic anhydrases and aromatic sulfonamides. *Biochemistry* **1970,** 9, 2638-45.
9. King, R. W.; Burgen, A. S. V. Kinetic Aspects of Structure-Activity Relations: The Binding of Sulphonamides by Carbonic Anhydrase. *Proceedings of the Royal Society B: Biological Sciences* **1976,** 193, 107-125.
10. Gao, J.; Qiao, S.; Whitesides, G. M. Increasing Binding Constants of Ligands to Carbonic Anhydrase by Using "Greasy Tails". *Journal of Medicinal Chemistry* **1995,** 38, 2292-2301.
11. Mecinovic, J.; Snyder, P. W.; Mirica, K. A.; Bai, S.; Mack, E. T.; Kwant, R. L.; Moustakas, D. T.; Heroux, A.; Whitesides, G. M. Fluoroalkyl and alkyl chains have similar hydrophobicities in binding to the "hydrophobic wall" of carbonic anhydrase. *J Am Chem Soc* **2011,** 133, 14017-26.

12. Snyder, P. W.; Mecinovic, J.; Moustakas, D. T.; Thomas, S. W., 3rd; Harder, M.; Mack, E. T.; Lockett, M. R.; Heroux, A.; Sherman, W.; Whitesides, G. M. Mechanism of the hydrophobic effect in the biomolecular recognition of arylsulfonamides by carbonic anhydrase. *Proceedings of the National Academy of Sciences of the United States of America* **2011,** 108, 17889-17894.
13. Kockar, F.; Maresca, A.; Aydın, M.; Işık, S.; Turkoglu, S.; Sinan, S.; Arslan, O.; Güler, Ö. Ö.; Turan, Y.; Supuran, C. T. Mutation of Phe91 to Asn in human carbonic anhydrase I unexpectedly enhanced both catalytic activity and affinity for sulfonamide inhibitors. *Bioorganic & Medicinal Chemistry* **2010,** 18, 5498-5503.
14. Schmid, M.; Nogueira, E. S.; Monnard, F. W.; Ward, T. R.; Meuwly, M. Arylsulfonamides as inhibitors for carbonic anhydrase: prediction & validation. *Chem. Sci.* **2012,** 3, 690-700.
15. Turkoglu, S.; Maresca, A.; Alper, M.; Kockar, F.; Işık, S.; Sinan, S.; Ozensoy, O.; Arslan, O.; Supuran, C. T. Mutation of active site residues Asn67 to Ile, Gln92 to Val and Leu204 to Ser in human carbonic anhydrase II: Influences on the catalytic activity and affinity for inhibitors. *Bioorganic & Medicinal Chemistry* **2012,** 20, 2208-2213.
16. Pacchiano, F.; Aggarwal, M.; Avvaru, B. S.; Robbins, A. H.; Scozzafava, A.; McKenna, R.; Supuran, C. T. Selective hydrophobic pocket binding observed within the carbonic anhydrase II active site accommodate different 4-substituted-ureido-benzenesulfonamides and correlate to inhibitor potency. *Chemical Communications* **2010,** 46, 8371-8373.
17. Hen, N.; Bialer, M.; Yagen, B.; Maresca, A.; Aggarwal, M.; Robbins, A. H.; McKenna, R.; Scozzafava, A.; Supuran, C. T. Anticonvulsant 4-Aminobenzenesulfonamide Derivatives with Branched-Alkylamide Moieties: X-ray Crystallography and Inhibition Studies of Human Carbonic Anhydrase Isoforms I, II, VII, and XIV. *Journal of Medicinal Chemistry* **2011,** 54, 3977-3981.
18. Avvaru, B. S.; Wagner, J. M.; Maresca, A.; Scozzafava, A.; Robbins, A. H.; Supuran, C. T.; McKenna, R. Carbonic anhydrase inhibitors. The X-ray crystal structure of human isoform II in adduct with an adamantyl analogue of acetazolamide resides in a less utilized binding pocket than most hydrophobic inhibitors. *Bioorganic & Medicinal Chemistry Letters* **2010,** 20, 4376-4381.
19. De Simone, G.; Alterio, V.; Supuran, C. T. Exploiting the hydrophobic and hydrophilic binding sites for designing carbonic anhydrase inhibitors. *Expert Opinion on Drug Discovery* **2013,** 8, 793-810.
20. Kanamori, K.; Roberts, J. D. Nitrogen-15 nuclear magnetic resonance study of benzenesulfonamide and cyanate binding to carbonic anhydrase. *Biochemistry* **1983,** 22, 2658-2664.
21. Fisher, S. Z.; Aggarwal, M.; Kovalevsky, A. Y.; Silverman, D. N.; McKenna, R. Neutron diffraction of acetazolamide-bound human carbonic anhydrase II reveals atomic details of drug binding. *Journal of the American Chemical Society* **2012,** 134, 14726-14729.
22. Kiefer, L. L.; Paterno, S. A.; Fierke, C. A. Hydrogen bond network in the metal binding site of carbonic anhydrase enhances zinc affinity and catalytic efficiency. *Journal of the American Chemical Society* **1995,** 117, 6831-6837.
23. Taylor, P. W.; King, R. W.; Burgen, A. S. Influence of pH on the kinetics of complex formation between aromatic sulfonamides and human carbonic anhydrase. *Biochemistry* **1970,** 9, 3894-902.

24. Eriksson, A. E.; Jones, T. A.; Liljas, A. Refined structure of human carbonic anhydrase II at 2.0 A resolution. *Proteins* **1988,** 4, 274-282.
25. Boriack, P. A.; Christianson, D. W.; Kingery-Wood, J.; Whitesides, G. M. Secondary Interactions Significantly Removed from the Sulfonamide Binding Pocket of Carbonic Anhydrase II Influence Inhibitor Binding Constants. *Journal of Medicinal Chemistry* **1995,** 38, 2286-2291.
26. Scott, A. D.; Phillips, C.; Alex, A.; Flocco, M.; Bent, A.; Randall, A.; O'Brien, R.; Damian, L.; Jones, L. H. Thermodynamic optimisation in drug discovery: a case study using carbonic anhydrase inhibitors. *ChemMedChem* **2009,** 4, 1985-9.
27. Martin, D. P.; Hann, Z. S.; Cohen, S. M. Metalloprotein–Inhibitor Binding: Human Carbonic Anhydrase II as a Model for Probing Metal–Ligand Interactions in a Metalloprotein Active Site. *Inorganic Chemistry* **2013,** 52, 12207-12215.
28. van Holde, K. E. A hypothesis concerning diffusion-limited protein–ligand interactions. *Biophysical Chemistry* **2002,** 101–102, 249-254.
29. Supuran, C. T. How many carbonic anhydrase inhibition mechanisms exist? *Journal of Enzyme Inhibition and Medicinal Chemistry* **2015**, 1-16.
30. Nair, S. K.; Ludwig, P. A.; Christianson, D. W. Two-Site Binding of Phenol in the Active Site of Human Carbonic Anhydrase II: Structural Implications for Substrate Association. *Journal of the American Chemical Society* **1994,** 116, 3659-3660.
31. Maresca, A.; Temperini, C.; Pochet, L.; Masereel, B.; Scozzafava, A.; Supuran, C. T. Deciphering the Mechanism of Carbonic Anhydrase Inhibition with Coumarins and Thiocoumarins. *Journal of Medicinal Chemistry* **2010,** 53, 335-344.
32. Maresca, A.; Temperini, C.; Vu, H.; Pham, N. B.; Poulsen, S.-A.; Scozzafava, A.; Quinn, R. J.; Supuran, C. T. Non-Zinc Mediated Inhibition of Carbonic Anhydrases: Coumarins Are a New Class of Suicide Inhibitors#. *Journal of the American Chemical Society* **2009,** 131, 3057-3062.
33. Davis, R. A.; Vullo, D.; Supuran, C. T.; Poulsen, S.-A. Natural Product Polyamines That Inhibit Human Carbonic Anhydrases. *BioMed Research International* **2014,** 2014, 6.
34. Tanc, M.; Carta, F.; Bozdag, M.; Scozzafava, A.; Supuran, C. T. 7-Substituted-sulfocoumarins are isoform-selective, potent carbonic anhydrase II inhibitors. *Bioorganic & Medicinal Chemistry* **2013,** 21, 4502-4510.
35. Tars, K.; Vullo, D.; Kazaks, A.; Leitans, J.; Lends, A.; Grandane, A.; Zalubovskis, R.; Scozzafava, A.; Supuran, C. T. Sulfocoumarins (1,2-Benzoxathiine-2,2-dioxides): A Class of Potent and Isoform-Selective Inhibitors of Tumor-Associated Carbonic Anhydrases. *Journal of Medicinal Chemistry* **2013,** 56, 293-300.
36. Innocenti, A.; Beyza Öztürk Sarıkaya, S.; Gülçin, İ.; Supuran, C. T. Carbonic anhydrase inhibitors. Inhibition of mammalian isoforms I–XIV with a series of natural product polyphenols and phenolic acids. *Bioorganic & Medicinal Chemistry* **2010,** 18, 2159-2164.
37. Innocenti, A.; Vullo, D.; Scozzafava, A.; Supuran, C. T. Carbonic anhydrase inhibitors: Interactions of phenols with the 12 catalytically active mammalian isoforms (CA I–XIV). *Bioorganic & Medicinal Chemistry Letters* **2008,** 18, 1583-1587.
38. Martin, D. P.; Cohen, S. M. Nucleophile recognition as an alternative inhibition mode for benzoic acid based carbonic anhydrase inhibitors. *Chemical Communications* **2012,** 48, 5259-5261.

39. Carta, F.; Temperini, C.; Innocenti, A.; Scozzafava, A.; Kaila, K.; Supuran, C. T. Polyamines Inhibit Carbonic Anhydrases by Anchoring to the Zinc-Coordinated Water Molecule. *Journal of Medicinal Chemistry* **2010,** 53, 5511-5522.
40. Reynolds, J. A.; Gilbert, D. B.; Tanford, C. Empirical correlation between hydrophobic free energy and aqueous cavity surface area. *Proceedings of the National Academy of Sciences of the United States of America* **1974,** 71, 2925-7.
41. Tanford, C. The hydrophobic effect and the organization of living matter. *Science* **1978,** 200, 1012-1018.
42. Hornak, V.; Abel, R.; Okur, A.; Strockbine, B.; Roitberg, A.; Simmerling, C. Comparison of multiple Amber force fields and development of improved protein backbone parameters. *Proteins* **2006,** 65, 712-725.
43. Peters, M. B.; Yang, Y.; Wang, B.; Füsti-Molnár, L. s.; Weaver, M. N.; Merz, K. M. Structural Survey of Zinc-Containing Proteins and Development of the Zinc AMBER Force Field (ZAFF). *J. Chem. Theory Comput.* **2010,** 6, 2935-2947.
44. Wang, J.; Wolf, R. M.; Caldwell, J. W.; Kollman, P. A.; Case, D. A. Development and testing of a general amber force field. *Journal of Computational Chemistry* **2004,** 25, 1157-1174.
45. Bayly, C. I.; Cieplak, P.; Cornell, W.; Kollman, P. A. A well-behaved electrostatic potential based method using charge restraints for deriving atomic charges: the RESP model. *Journal of Physical Chemistry* **1993,** 97, 10269-10280.
46. *Macromodel*, 9.9; Schrödinger, LLC: New York, 2012.
47. Jorgensen, W. L.; Tirado-Rives, J. The OPLS [optimized potentials for liquid simulations] potential functions for proteins, energy minimizations for crystals of cyclic peptides and crambin. *Journal of the American Chemical Society* **1988,** 110, 1657-1666.
48. Jorgensen, W. L.; Maxwell, D. S.; Tirado-Rives, J. Development and Testing of the OPLS All-Atom Force Field on Conformational Energetics and Properties of Organic Liquids. *Journal of the American Chemical Society* **1996,** 118, 11225-11236.
49. Pronk, S.; Páll, S.; Schulz, R.; Larsson, P.; Bjelkmar, P.; Apostolov, R.; Shirts, M. R.; Smith, J. C.; Kasson, P. M.; van der Spoel, D.; Hess, B.; Lindahl, E. GROMACS 4.5: a high-throughput and highly parallel open source molecular simulation toolkit. *Bioinformatics* **2013**.
50. Parrinello, M.; Rahman, A. Polymorphic transitions in single crystals: A new molecular dynamics method. *Journal of Applied Physics* **1981,** 52, 7182-7190.
51. Bussi, G.; Donadio, D.; Parrinello, M. Canonical sampling through velocity rescaling. *Journal of Chemical Physics* **2007,** 126, 014101.
52. Barducci, A.; Bussi, G.; Parrinello, M. Well-Tempered Metadynamics: A Smoothly Converging and Tunable Free-Energy Method. *Physical Review Letters* **2008,** 100, 020603.
53. Bonomi, M.; Branduardi, D.; Bussi, G.; Camilloni, C.; Provasi, D.; Raiteri, P.; Donadio, D.; Marinelli, F.; Pietrucci, F.; Broglia, R. A.; Parrinello, M. PLUMED: A portable plugin for free-energy calculations with molecular dynamics. *Computer Physics Communications* **2009,** 180, 1961-1972.
54. Daura, X.; Gademann, K.; Jaun, B.; Seebach, D.; van Gunsteren, W. F.; Mark, A. E. Peptide Folding: When Simulation Meets Experiment. *Angewandte Chemie International Edition* **1999,** 38, 236-240.
55. Rocchia, W.; Alexov, E.; Honig, B. Extending the Applicability of the Nonlinear Poisson−Boltzmann Equation: Multiple Dielectric Constants and Multivalent Ions†. *Journal of Physical Chemistry B* **2001,** 105, 6507-6514.

56. Dovesi, R.; Orlando, R.; Erba, A.; Zicovich-Wilson, C. M.; Civalleri, B.; Casassa, S.; Maschio, L.; Ferrabone, M.; De La Pierre, M.; D'Arco, P.; Noël, Y.; Causà, M.; Rérat, M.; Kirtman, B. CRYSTAL14: A program for the ab initio investigation of crystalline solids. *International Journal of Quantum Chemistry* **2014,** 114, 1287-1317.
57. http://www.crystal.unito.it/basis-sets.php
58. Hutter, J.; Iannuzzi, M.; Schiffmann, F.; VandeVondele, J. cp2k: atomistic simulations of condensed matter systems. *WIREs Comput. Mol. Sci.* **2014,** 4, 15-25.
59. Goedecker, S.; Teter, M.; Hutter, J. Separable dual-space Gaussian pseudopotentials. *Phys. Rev. B* **1996,** 54, 1703-1710.
60. VandeVondele, J.; Hutter, J. Gaussian basis sets for accurate calculations on molecular systems in gas and condensed phases. *Journal of Chemical Physics* **2007,** 127, 114105-114105.
61. Myszka, D. G. Analysis of small-molecule interactions using Biacore S51 technology. *Anal. Biochem.* **2004,** 329, 316-323.
62. Mueller, U.; Darowski, N.; Fuchs, M. R.; Forster, R.; Hellmig, M.; Paithankar, K. S.; Puhringer, S.; Steffien, M.; Zocher, G.; Weiss, M. S. Facilities for macromolecular crystallography at the Helmholtz-Zentrum Berlin. *J Synchrotron Radiat* **2012,** 19, 442-9.
63. Kabsch, W. Xds. *Acta Crystallogr D Biol Crystallogr* **2010,** 66, 125-32.
64. McCoy, A. J.; Grosse-Kunstleve, R. W.; Adams, P. D.; Winn, M. D.; Storoni, L. C.; Read, R. J. Phaser crystallographic software. *J Appl Crystallogr* **2007,** 40, 658-674.
65. Project, C. C. The CCP4 suite: programs for protein crystallography. *Acta Crystallograph. D* **1994,** 50, 760-763.
66. Lesburg, C. A., Christianson, D.W. X-Ray Crystallographic Studies of Engineered Hydrogen Bond Networks in a Protein-Zinc Binding Site. *J.Am.Chem.Soc* **1995,** 117, 6838-6844.
67. Adams, P. D.; Afonine, P. V.; Bunkoczi, G.; Chen, V. B.; Davis, I. W.; Echols, N.; Headd, J. J.; Hung, L.-W.; Kapral, G. J.; Grosse-Kunstleve, R. W.; McCoy, A. J.; Moriarty, N. W.; Oeffner, R.; Read, R. J.; Richardson, D. C.; Richardson, J. S.; Terwilliger, T. C.; Zwart, P. H. PHENIX: a comprehensive Python-based system for macromolecular structure solution. *Acta Crystallograph. D* **2010,** 66, 213-221.
68. Emsley, P.; Cowtan, K. Coot: model-building tools for molecular graphics. *Acta Crystallogr D Biol Crystallogr* **2004,** 60, 2126-32.
69. O. S. Smart; T. O. Womack; A. Sharff; C. Flensburg; P. Keller; W. Paciorek; C. Vonrhein; Bricogne., G. *Grade*, Vol. 2014; Global Phasing Ltd.: Cambridge, 2014.
70. Laskowski, R. A.; MacArthur, M. W.; Moss, D. S.; Thornton, J. M. PROCHECK: a program to check the stereochemical quality of protein structures. *J. Appl.Crystallogr.* **1993,** 26, 283-291.

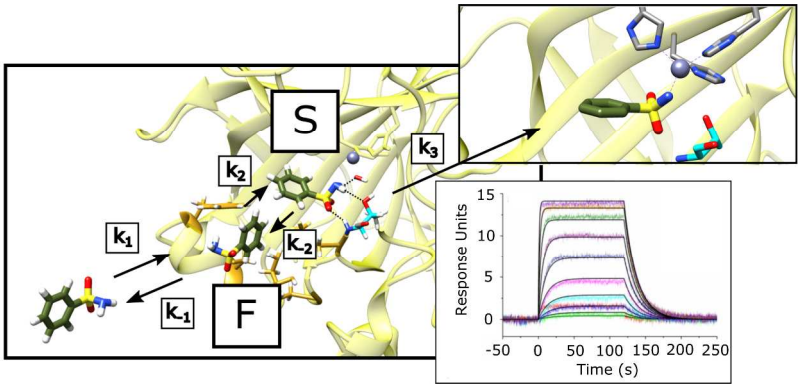
S
F
k1
k-1
k2
k-2
k3
Response Units
15
10
5
0
-50
0
50
100
150
200
250
Time (s)